crystal phonon spectrum.[16]

(iv) Since the renormalization ΔE is asymptotically of order $1/Z$, we add to the CPA corrections of order $1/Z^n$, $n=1,2,\cdots$. According to recent discussions,[4,17] we expect to have at least the same number of exact moments, i.e., eight. Our density of states will have to intersect at least eight times the CPA density of states. This can be seen on our numerical results.

Though somewhat more tedious, the iterative calculation is not in principle more complicated than in CPA and does not require the introduction of a small imaginary part. We did not meet the analyticity difficulty reported in some one-dimension calculations of pair effects.[7] The only problem seems to be the possible occurrence of a pole in the self-energy $\Sigma(z)$ at $z=-\bar{E}=-[xE_A+(1-x)E_B]$. For the exact averaged Green's function, it has been proved[2] that this pole always occurs in the band gaps. In the CPA, the pole may occur before the exact subbands are split, depending on the model density of states, but always lies outside the narrower CPA bands. In the BPA, since the bands are broader than in CPA, this pole can appear in a nonzero density-of-states region and gives in some cases at $E=-\bar{E}$ a narrow unphysical gap.

In conclusion, we think that this approach, without increasing too much the computational difficulties, yields more precise results on the shape of the density of states and can be of valuable interest in all problems, namely, magnetic, when the local density of states is of primary importance.

We want to thank J. Van der Rest for help in the preparation of numerical calculations.

*Laboratoire associé au CNRS.
[1]P. Soven, Phys. Rev. **156**, 809 (1967).
[2]B. Velicky, S. Kirkpatrick, and H. Ehrenreich, Phys. Rev. **175**, 747 (1968).
[3]B. Nickel and J. A. Krumhansl, Phys. Rev. B **4**, 4354 (1971).
[4]L. Schwartz and E. Siggia, Phys. Rev. B **5**, 383 (1972).
[5]F. Cyrot-Lackman and F. Ducastelle, Phys. Rev. Lett. **27**, 1429 (1971).
[6]F. Cyrot-Lackman and M. Cyrot, J. Phys. C 5, L209 (1972).
[7]B. Nickel (private communication).
[8]H. A. Bethe, Proc. R. Soc. Lond. **150**, 552 (1935).
[9]K. M. Watson, Phys. Rev. **105**, 1388 (1957).
[10]P. W. Anderson, Phys. Rev. **109**, 1492 (1958).
[11]J. M. Ziman, J. Phys. C **2**, 1230 (1969).
[12]D. J. Thouless, in Proceedings of the Fifth International Conference on Amorphous and Liquid Semiconductors, Ann Arbor, Mich., 1971 (unpublished).
[13]C. Domb, Adv. Phys. **9**, 149 (1960).
[14]L. Schwartz, F. Brouers, A. V. Vedyayev, and H. Ehrenreich, Phys. Rev. B **4**, 3383 (1971).
[15]W. Butler, Phys. Lett. A **39**, 203 (1972).
[16]D. W. Taylor, Phys. Rev. **156**, 1017 (1967).
[17]F. Brouers and A. V. Vedyayev, J. Phys. F 3, 127 (1973).

PHYSICAL REVIEW B VOLUME 7, NUMBER 10 15 MAY 1973

Cyclotron Resonance in Tellurium

Y. Couder, M. Hulin, and H. Thomé
Laboratoire de Physique des Solides de l'Ecole Normale Supérieure,*
24 rue Lhomond, Paris V, France
(Received 6 July 1972)

Cyclotron resonance experiments in tellurium carried out over a wide and continuous range of microwave frequencies are described and analyzed; the influence of temperature and of the orientation of the magnetic field with respect to the crystallographic axes received particular attention. All the results are consistent with a $\vec{k}\cdot\vec{p}$ perturbation model of the valence band structure. We determined the parameters of this model and find a quantitative agreement between theory and experiments.

I. INTRODUCTION

The first cyclotron resonance experiments in tellurium were performed at low frequency by Mendum and Dexter[1] working at $\lambda=4$ mm and by Picard[2] at $\lambda=0.9$ mm, and were in agreement with a conventional ellipsoidal model of the isoenergetic surfaces. However, in the first experiments at higher frequencies[3] we found a splitting of the cyclotron resonance line in the $\vec{B}\perp\vec{c}$ direction, and we showed that this feature was in good agreement with the theoretical model of Hulin,[4,5] in which the valence-band maximum is close to the corner of the Brillouin zone giving a "camel back" shape to the top of the band. Betbeder and Hulin,[6] among others, calculated the forked shape of the Landau levels in that case.

Cyclotron resonance experiments were then performed at higher frequencies by Dreybrodt *et al.*[7,8] using a cyanide laser ($\lambda=337\ \mu$, $\lambda=195\ \mu$). Yoshizaki and Tanaka,[9] working with a monochromator, reached the wavelength range $300\mu>\lambda>80\ \mu$. A

large number of new transitions were observed; however, although they were interpreted using qualitatively similar models of the band structure, there remain quantitative divergencies between the values of band parameters that have been put forward by different authors. Essentially this is due to the strong nonparabolicity of the valence band near its maximum, which in turn leads to a complicated and violently nonlinear dependence of the Landau energies on the magnetic field: In such conditions, it is difficult to ascribe nonambiguously the observed absorption maxima to definite transitions between Landau levels.

We present here the results of experiments performed over a large range of frequencies ($0.3 < \lambda < 4$ mm) at temperatures $1.5\,^{\circ}\mathrm{K} < T < 30\,^{\circ}\mathrm{K}$. A splitting of the Landau levels $n = 0^{\pm}$, $n = 1^{\pm}$, $n = 2^{\pm}$, is directly observed: Semiclassically, it can be described as resulting from intravalley magnetic breakdown inside the valence band; a complete description of the first Landau levels can be deduced from the experiments. This allows a precise determination of the band parameters.

Transitions due to impurity levels are also observed and interpreted. Finally, we present the results and the interpretation of experiments performed with the magnetic field along all the intermediate directions between the c axis and the bisector axis. These experiments, which in particular show up very clearly how the splitting of the cyclotron resonance line appears when the angle between the magnetic field and the c axis approaches 90°, bring a supplementary confirmation of the valence band parameters.

II. SUMMARY OF PREVIOUS THEORETICAL RESULTS

A. General Features of the Valence Band

The valence band of trigonal tellurium has been studied through a number of experimental techniques (cyclotron resonance,[1-9] Shubnikov–de Haas effect,[10-12] infrared absorption and magnetoabsorption,[13-14] and magnetophonon measurements[15]) which, together with theoretical investigation, have led to the adoption of the following semiempirical model (see Ref. 16 for a summary).

The top of the valence band lies in the vicinity of the corners H (an alternative notation is M[14,16,17]) of the Brillouin zone which has the form of a hexagonal prism. In the following, a corner H of the Brillouin zone will be taken as the origin in $\vec{k}$ space with orthogonal axes for the $\vec{k}$ components. (k_z is parallel to the trigonal $\vec{c}$ axis, k_x to a binary axis, k_y to the "bisector" direction between two binary axes.)

Owing to the influence of the spin-orbit interaction, there appears a set of two bands, originating at the nondegenerate levels H_4 and H_5, (an alternative notation is $\bar{M}_1$, $\bar{M}_1'$), the energies being given, to the lowest relevant order in $|\vec{k}|$, by the expression

$$E(\vec{k}) = -\alpha k_z^2 - \beta' k_\perp^2 \pm [(A + \beta' \eta k_\perp^2)^2 + 4\alpha^2 \zeta^2 k_z^2]^{1/2} - C, \tag{1}$$

where

$$k_\perp^2 = k_x^2 + k_y^2, \quad C = \alpha\zeta^2 + A^2/4\alpha^2\zeta^2 ,$$

and the ± sign corresponds to the upper and lower bands, respectively.

In fact, we are only interested in the upper valence band. For the values of the band parameters that are suggested by previous studies,[10,13] (1) then reduces to

$$E = -\alpha k_z^2 - \beta k_\perp^2 + (A^2 + 4\alpha^2\zeta^2 k_z^2)^{1/2} - C , \tag{2}$$

where

$$\beta = \beta'(1 - \eta/t_0), \quad t_0 = 2\alpha\zeta^2/A$$

without any significant loss of precision.

Perhaps we should point out here that Eqs. (1) and (2) take no account of terms in $|\vec{k}|^3$, $|\vec{k}|^4$ and so on, which have formally been introduced by other authors[17]: Such terms do not lend themselves to a quantitative treatment (for instance, in the determination of Landau levels) so, in the following, we shall only give qualitative indications on their influence. (Similarly, we have ignored additional spin effects which have been shown to be of negligible importance.[17])

In (1) and (2), the origin for electron energies is taken at the top of the valence band, which corresponds to two-band maxima lying at $k_z = \pm k_{z0}$ on the k_z axis. At $k_z = k_\perp = 0$, there appears a saddle point in the band structure (state H_4), owing to the camelback shape of the upper band $E(k_z;\ k_\perp = 0)$ (Fig. 1).

We can profit by the rotational invariance of the isoenergetic surfaces around the k_z axis to complement Fig. 1 by showing E as a function of k_z and $k_\perp$ (Fig. 2). This representation will prove useful in the following discussion.

We shall call (Δ) the energy difference between the band maxima and the saddle point:

$$\Delta = C - A = \alpha\zeta^2(1 - A/2\alpha\zeta^2)^2 . \tag{3}$$

Previous analysis of experimental results have yielded: (a) a precise value, $2A = 126.1 \pm 0.2$ meV, of the spin-orbit splitting between H_4 and H_5; this figure, which is obtained from infrared absorption studies, will be directly entered in the calculations. (b) A value for Δ ranging from 2–2.5 meV,[14,15,17] which we shall redetermine here, but on the order of magnitude of which we shall rely in the following discussion.

B. Landau Levels

The Landau quantization corresponding to this band structure has been investigated by several

authors.[5-9,16-18] Let us summarize the main results corresponding to the simplest orientations of the magnetic field $\vec{B}$ with respect to the crystallographic directions. (From now on, we shall reverse the sign of electron energies, which amounts to evaluating *hole energies*, the origin being still taken at the top of the valence band.)

(i) $\vec{B} \parallel \vec{c}$ *axis*. k_z remains a good quantum number; owing to the quadratic dependence of E vs $k_\perp$ in (2), the Landau quantization assumes the classical form corresponding to parabolic bands, the energy for the nth Landau level being

$$E_n(k_z) = [\alpha k_z^2 (A^2 + 4\alpha^2 \zeta^2 k_z^2)^{1/2} + C] + (n + \tfrac{1}{2})\,\hbar\omega_c$$
$$\hbar\omega_c = 2\beta eB/\hbar = \hbar(eB/m_\parallel), \quad m_\parallel = \hbar^2/2\beta . \tag{4}$$

Electric dipole transitions under the influence of a rf field are allowed only for $\Delta n = \pm 1$, so one expects to find essentially a classical cyclotron resonance line for a frequency $\omega = \omega_c$, the ratio ω/B directly yielding the value of β.

Let us remark that including higher order terms in (2) would lead to the possible appearance of harmonics, and introduce a slight dependence of $\hbar\omega_c$ with k_z. At low temperatures however (e.g., for $kT < \Delta$, that is $T \lesssim 20\,^\circ$K) only the vicinity of the band maxima is populated with holes, so that one should essentially measure the transverse effective mass $m_\parallel$ for $|k_z| = k_{z_0}$. This conclusion is enhanced when one takes into account the smearing

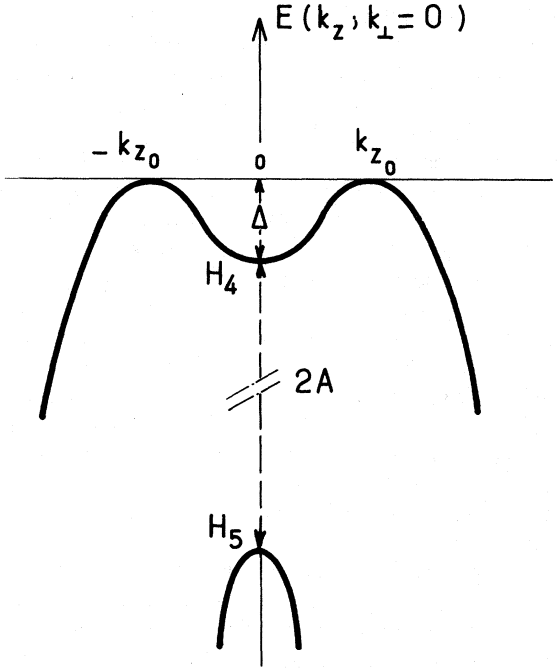

FIG. 1. Schematic band structure of tellurium. (The wave vector origin is taken at the corner of the Brillouin zone.)

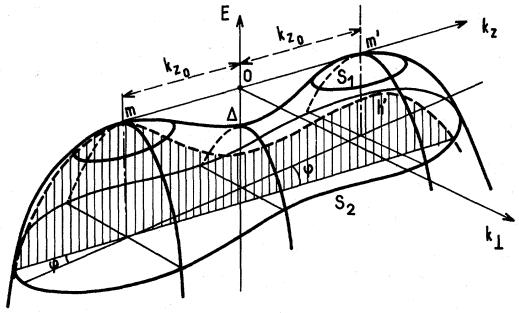

FIG. 2. $E(k_z, k_\perp)$ surface near the top of the valence band. Notice the semiclassical trajectories (S_1 and S_2) in a magnetic field perpendicular to the c axis for cyclotron energies below and above Δ. The shaded region indicates the shape of the effective potential curve for holes moving in a magnetic field tilted by an angle φ from the binary axis (cf. Sec. V).

out of the singular points in the density of states by collision broadening.[19]

(ii) $\vec{B} \perp \vec{c}$ *axis*. Let us for instance take $\vec{B} \parallel \vec{k}_y$ (bisector direction). It has been shown[6] that the Landau levels can be determined starting from the eigenstates for an electron moving in a one dimensional "effective" potential $V(X)$, which reproduces the camel-back curve on Fig. 1, but for a change in the scales of (a) the abscissa X, which is given by the transformation $k_z \to (\beta/\alpha)^{1/4}\,(eB/\hbar)^{1/2}\,X$, and (b) the energy, which is referred to the "unit" $E_0 = (\alpha\beta)^{1/2}\,(eB/\hbar)$. Ultimately, the Landau energy E will be derived from the eigenvalue ϵ of the Schrödinger equation

$$-\frac{d^2\psi}{dX^2} + V(X)\psi = \epsilon\psi ,$$

with

$$V(X) = X^2 - (\bar{A}^2 + 4\xi^2 X^2)^{1/2} + \bar{C} , \tag{5}$$

where

$$\bar{A} = A/E_0, \quad \bar{C} = C/E_0, \quad \xi = (\alpha/\beta)^{1/4}\,(eB/\hbar)^{-1/2}\,\zeta$$

through the relation

$$E = E_0\epsilon + \beta k_y^2 . \tag{6}$$

The eigenstates ψ of (5), owing to the invariance of $V(X)$ under the inversion $X \to -X$, are either even or odd in X. They will accordingly be labeled by the index $n^\pm$ ($n = 0, 1, 2\ldots$) and appear, when taken for increasing values of ϵ, in the order, 0^+, 0^-, 1^+, 1^-, $2^+\ldots$.

The essential features of the energy spectrum in this situation are the following[6,16]:

(a) For low values of B, the effective potential $V(X)$ presents two deep, well separated, symmetrical potential wells, with minima at

$$X = \pm X_0, \quad X_0 = (\beta/\alpha)^{-1/4}\,(eB/\hbar)^{-1/2}\,k_{z_0}$$

(so that X_0 is actually large for small B). The height of the barrier between these wells is $\bar{\Delta} = \Delta/E_0 \propto B^{-1}\Delta$ (which accordingly increases as B decreases) (Fig. 3).

To each valley, which is nearly isolated from its neighbor, there corresponds a series of wave functions, $\psi_n(X - X_0)$ or $\psi_n(X + X_0)$ with identical energies $\epsilon_n = (n + \frac{1}{2})\hbar\omega_c$ ($n = 0, 1\ldots$) closely resembling those of a harmonic oscillator (at least for n small enough to verify $\epsilon_n \ll \bar{\Delta}$), the spacing $\hbar\omega_c$, which will yield the cyclotron energy $\hbar\omega_c$ after multiplication by E_0, being determined by the curvature of $V(X)$ at $X = \pm X_0$, a quantity which is readily shown to be independent of B, as well as $\hbar\omega_c$ itself. Actually, there is a small interaction between the two valleys, through the barrier: The eigenfunctions $\psi_{n^\pm}$, however, do not differ appreciably from the (anti)symmetric linear combinations

$$\psi_{n^\pm} \approx 2^{-1/2}[\psi_n(X - X_0) \pm \psi_n(X + X_0)]$$

and the degeneracy—for sufficiently small n—is nearly unaffected, so that we can take

$$\epsilon_{n^\pm} \approx \epsilon_n .$$

Consequently, the hole energy spectrum itself exhibits a twofold degeneracy and a linear dependence on the magnetic field and we can write

$$E_{n^\pm} = E_0\epsilon_{n^\pm} \approx E_0\epsilon_n = (n + \tfrac{1}{2})\,(\hbar eB/m_c)\,, \qquad (7)$$

where $m_c = (m_\parallel m_\perp)^{1/2}$ is the appropriate cyclotron effective mass associated to the nearly parabolic parts of $V(X)$ near its maxima.

(b) When B increases, both X_0 and $\bar{\Delta}$ decrease, and the interaction between levels associated with both valleys increases, this coupling being felt the sooner the higher the value of n.

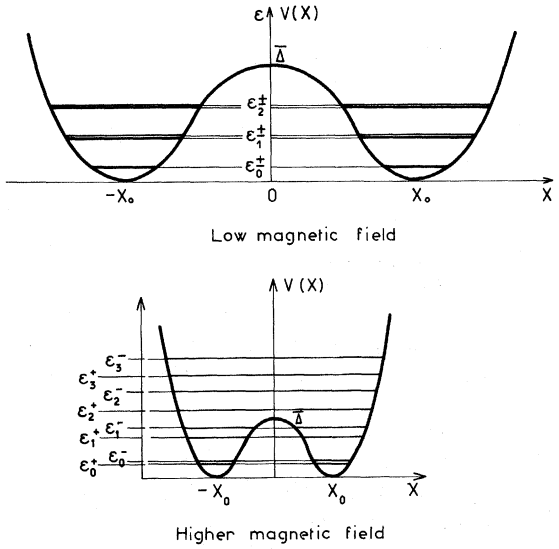

FIG. 3. Landau levels at low and high magnetic field (B parallel to bisector axis).

The previously observed degeneracy between even and odd levels is progressively removed, first for high values of n, then for $n = 2$, $n = 1$ and finally $n = 0$, as the corresponding ϵ_n becomes comparable with $\bar{\Delta}$.

As a result, the curves $E_{n^\pm}(B)$, which are not distinguished for low values of B, progressively separate one from the other, finally yielding the characteristic pattern which will be shown on Fig. 9 in relation with the interpretation of the experimental results. All these results can be interpreted in a semiclassical scheme taking account of possible magnetic breakdown (Ruvalds and McClure[12,15,20]). For $\hbar\omega_c \lesssim \Delta$, the semiclassical trajectories are quasielliptic (curve S_1 on Fig. 2), hence the conventional linear dependence of ω_c with B for low enough magnetic fields.

For $\hbar\omega_c \gtrsim \Delta$, the semiclassical trajectories look like curve S_2 on Fig. 2: They correspond to the junction of two of the previous ellipses. The quasiclassical quantization rule on the area inside the curve here involves an area which is approximately twice that of an isolated ellipse. Hence we can predict that the energy distance between Landau levels will be approximately half that which would be obtained by extrapolating the results obtained for small B; this corresponds to the removal of the degeneracy between + and − states. In this process, all levels keep a definite parity with respect to the reversal of X. It can be shown[6] that electric-dipole transitions should couple levels with opposite parities (e.g. $0^+ \rightarrow 1^-, 0^- \rightarrow 1^+$). This follows from the fact that the perturbation Hamiltonian of the rf field is itself *odd* with respect to the transformation $X \rightarrow -X$, since it appears, apart from some constant factor, either as X or $\partial/\partial X$ depending on the polarization, so that its matrix elements vanish between eigenfunctions $\psi_{n^\pm}$ of identical symmetry properties. However, introducing higher order terms in $\vec{k}$ in the dispersion equation (2) and the corresponding Schrödinger equation (5) removes this selection rule. One should then be able to observe transitions such as $0^+ \rightarrow 1^+$, $0^- \rightarrow 1^-$, etc., although they can be expected to lead to weaker absorption peaks than the "fully allowed" transitions of the previous type. It should also be stressed that the classical harmonic oscillator selection rule $\Delta n = \pm 1$ no longer holds in this model, so that "harmonics" should appear in cyclotron resonance.

In addition, it should be indicated that previous studies[3,6,9,14,21] have shown that the foregoing description should be complemented by introducing impurity levels corresponding to maybe several acceptor states, the fundamental of which should lie at $E_0 = 1.3$–1.4 meV above the valence-band maxima (a figure which is supported by a variation-

al calculation within the effective-mass model[22]). When a magnetic field is applied, this level should essentially follow the zero Landau level, with a slight possible variation of the ionization energy E_0 with B. The presence of these levels naturally adds to the complexity of the energy spectrum and to the difficulty met in interpreting cyclotron resonance experiments.

Thus, while preliminary investigations[3] have revealed the characteristic "branching phenomenon" due, for instance, to the separation of levels 1^+ and 1^- for sufficiently high magnetic fields, the improvement of experimental techniques naturally leads to an increasing complexity of the absorption spectrum, and makes it necessary to exercise much care in the attribution of the observed lines to definite transitions. This can only be done by a precise investigation of these lines through a wide and, as much as possible, continuous range of magnetic fields and microwave frequencies, with constant reference to the theoretical model. The next sections will describe the present state of the fulfillment of this program.

III. EXPERIMENTAL SETUP

A. Samples

Whatever the preparation techniques used, all tellurium samples are extrinsic and p type. We used samples from two different origins: Ultrapure samples with hole concentration $p < 5\times10^{13}\,\mathrm{cm}^{-3}$ and samples doped with either bismuth or antimony with $p \sim 10^{14}\ \mathrm{cm}^{-3}$. The carrier mobility[23] is of the order of 100 000 $\mathrm{cm}^2/\mathrm{V\,sec}$ at $T = 1.5\,^\circ\mathrm{K}$. For $p \sim 10^{14}\ \mathrm{cm}^{-3}$ the plasma frequency $\omega_p \sim 50$ GHz is always smaller than our working frequency 130 GHz $< \omega <$ 1000 GHz.

Tellurium is well known for its pathological sensitivity to external mechanical treatments. The best samples are obtained by cleaving them along planes parallel to both the c and binary axes. We use small plates (5×5×1 mm) with the main surface containing both the c and binary axes, and perpendicular to a bisector axis.

B. Sources

For these experiments, we used a large number of different microwave sources; seven backward-wave "carcinotron" oscillators,[24,25] from Thomson-C. S. F. Co., emitting, respectively, in the wavelength ranges 2 mm, 1 mm, 900, 700, 600, 500, and 400 μ and a cyanide laser emitting at 337 or at 311 μ. The typical output power of the submillimetric carcinotrons is of the order of 20 mW and the emitted microwave is monochromatic. The stability in frequency and power is $\sim 10^{-4}$. By tuning the line voltage one can shift continuously the emitted frequency inside the emission band of the carcinotron, the typical broadness of which is $(\omega_{max} - \omega_{min})/\omega \sim 0.1$. Hence we could work at almost any wavelength λ between 400 μ and 1 mm. Two gaps in frequency separate these experiments from those at 2 mm on one side and from those at 337 μ on the other side.

C. Detection

The sample being reasonably transparent, a transmission technique is used. Special care must be taken in designing the sample holder (Fig. 4), which permits the heating of the sample up to temperatures $T \lesssim 30\,^\circ\mathrm{K}$. The sample holder is located at the end of the waveguide in a chamber filled with a low pressure of exchange gas. The increase of temperature of the sample holder is obtained by a heating wire and measured by a bolometer. The microwave power transmitted through the sample is measured by another bolometer (an Allen Bradley resistor reduced to a thickness of 0.3 mm) immersed in the superfluid helium bath beneath a Mylar window.

D. Magnetic Field

The experiments with $\vec{B}$ parallel to the bisector axis were performed in the Faraday geometry ($\vec{k} \parallel \vec{B}$) in the axial magnetic field of a superconducting coil which provides a field up to 58 kG.

For the other crystallographic directions, a Voigt configuration ($\vec{k} \perp \vec{B}$) was used. The sample plate is then vertical, parallel to the axial field of the coil, and can be rotated so as to investigate all the crystallographic directions contained in the plane of the sample, between the binary axis and the c axis. The microwave is polarized with $\vec{E} \perp \vec{B}$ by means of a grid. Other experiments were performed in the Voigt geometry using the transverse magnetic field of an electromagnet (for $B < 27.5$ kG).

IV. RESULTS AND DISCUSSION

The spectrum at low frequencies in both crystallographic directions, $\vec{B}$ parallel to the $\vec{c}$ axis and $\vec{B}$ parallel to the binary axis, is relatively simple. At higher frequency a large number of new absorption lines appear, which at first sight seem rather inextricable.

Characteristic recordings of the transmitted power as a function of magnetic field in the direction $\vec{B}$ parallel to the bisector axis at $T = 1.5\,^\circ\mathrm{K}$ are shown on Fig. 6.

The evolution of each line can be followed through the recordings performed at a large number of frequencies. Thanks to the wide frequency range covered by our microwave sources, a plot of the position of the lines in a $\omega(B)$ diagram can be drawn with accuracy. Figure 5 shows this plot for $\vec{B}$ parallel to the $\vec{c}$ axis, Fig. 8 for $\vec{B}$ parallel to

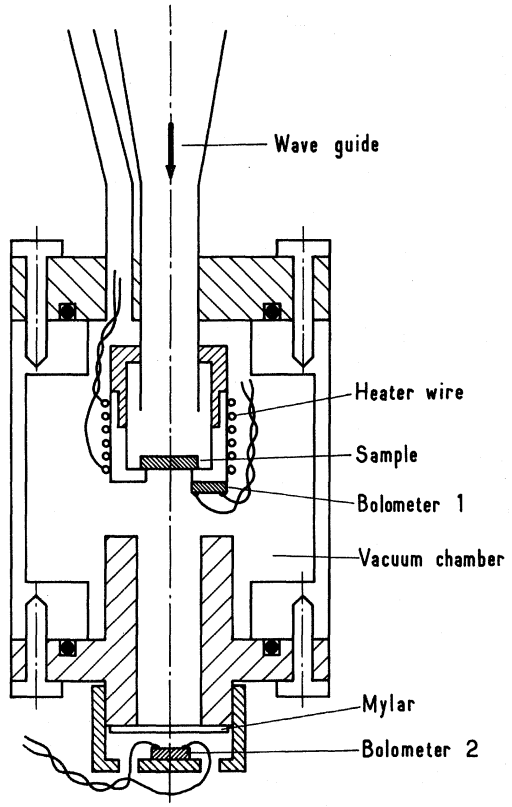

FIG. 4. Experimental arrangement. The sample holder is heated by heating wire. Bolometer (1) measures its temperature. The bolometer (2), which measures the transmitted microwave power, is immersed in the superfluid helium of the cryostat.

the bisector axis. At low temperature in both these diagrams the lines can be classified in three categories: (i) The position of the lines labeled F can be extrapolated to the origin $B=0$, $\omega=0$. (ii) The S lines parallel to the F lines in the $\omega(B)$ diagram extrapolate at $B=0$ to the same nonzero transition energy $\hbar\omega \sim 1.24$ meV. (iii) The I lines are very sharp ones, almost field independent.

The distinction between these three classes is confirmed by the experiments performed at increasing temperatures (Fig. 7). The intensity of the F lines increases together with their linewidth. The S (and I) lines disappear for a small increase of the temperature. We will see that they are related to impurity levels located above the valence band.

At higher temperatures new lines, that we shall call T, show up.

We first limit the discussion to the F and T lines (Sec. IV A). In Sec. IV B we study the S and I lines. We show that the F and T lines correspond to transitions between Landau levels, the S lines to transitions from an impurity level to a Landau level, and the I lines to transitions between two impurity levels.

A. Transitions between Landau Levels

(i) $\vec{B} \parallel \vec{c}$ *axis*. For the reasons discussed in Sec. III A, the experiments with $\vec{B}$ parallel to the $\vec{c}$ direction were performed with a cleaved sample in the Voigt geometry. The pure cyclotron resonance cannot then be observed even in a sample in which only one type of carrier contributes to the absorption. Instead, a magnetoplasma resonance occurs at frequency

$$\omega = (\omega_c^2 + \omega_p^2)^{1/2} \ .$$

In our samples the plasma frequency is $\omega_p \sim 50$ GHz, while the working frequency ω is >300 GHz. The position of the observed resonance thus differs only by a factor $\omega_p^2/2\omega_c^2 < 1.4\%$ from the cyclotron frequency ω_c.

The ω vs B dependence of the main resonance peak (F_c line) is linear at high frequency (Fig. 5). This is in good agreement with the parabolic $k_\perp$ dependence of the energy predicted by the theoretical model of Sec. II [cf. Eq. (4)].

The cyclotron resonance mass in this direction is

$$m_\parallel = (0.108 \pm 0.001) m_0 \ .$$

When the temperature of the sample is increased, the F_c resonance peak broadens but no other absorption maximum appears.

We did not observe the splitting of the F_c line

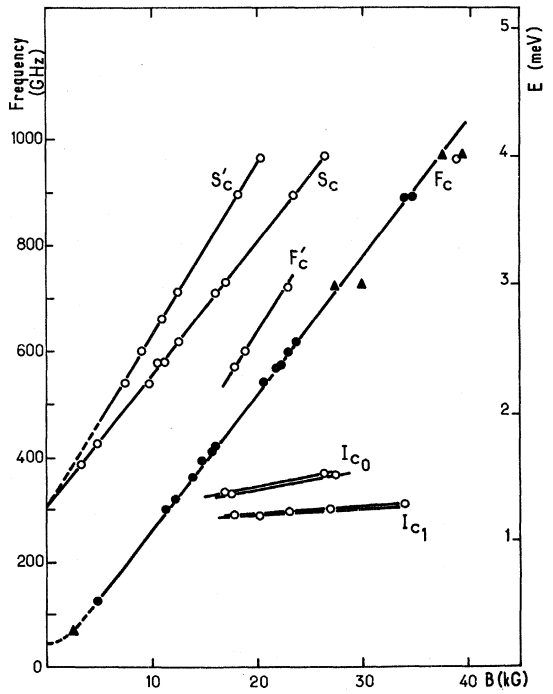

FIG. 5. Plot of the position of minima of transmission with $\vec{B} \parallel \vec{c}$ axis: ●, temperature independent lines; ○, lines observed at $T=1.5$ °K only; ▲, lines observed by Yoshizaki *et al.*

described by Yoskizaki *et al.*[9] in their work at higher frequency, and which they attributed to the existence of high-order terms in the k dependence of F. The cyclotron mass is then a function of k_z, and the two observed lines should correspond to the external masses at $|k_z| = k_{z_0}$ and $k_z = 0$. This interpretation has recently been criticized on theoretical grounds by Bangert and Dreybrodt[19]: It appears that the density of states for $k_z = 0$ is not sufficient to lead to an absorption peak when the finite relaxation time τ is taken into account. Perhaps the broadening of the F_c line which we noticed with increasing temperature arises from such nonparabolicity effects.

The two weak lines S_c' and F_c' which flank S_c and F_c have not been observed in all samples. They might be related to a stress effect on the sample.

(ii) $\vec{B} \perp \vec{c}$. The results we shall now describe and discuss were obtained in the Faraday configuration with $\vec{B}$ parallel to the bisector axis. Some experiments have also been performed in the Voigt geometry with $\vec{B}$ parallel to the binary axis; no significant difference could be observed, which confirms the limited importance of the trigonal warping of the band structure.

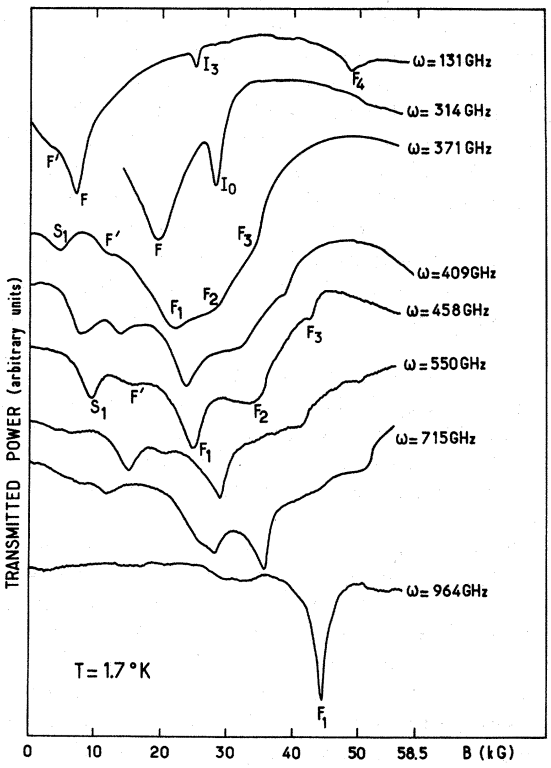

FIG. 6. Low temperature ($T = 1.5$ °K) cyclotron resonance absorption spectra in tellurium at various frequencies for $\vec{B}$ parallel to bisector axis. The recording at $\omega = 371$ GHz shows clearly the splitting of the line F into three lines F_1, F_2, and F_3.

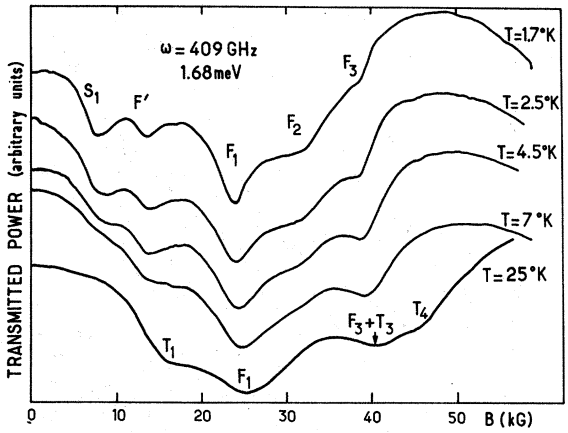

FIG. 7. Evolution of the cyclotron resonance spectrum with temperature at constant frequency ($\omega = 409$ GHz).

At low frequency ($\omega \sim 130$ GHz) the cyclotron resonance line F is quite intense (Fig. 6), and its linewidth is $\Delta B \sim 2000$ G. F is flanked by a weak line F'. At high magnetic field a new line F_4 shows up.

When the working microwave frequency is increased, the F line first broadens (at 315 GHz for instance $\Delta B \sim 3500$ G). At still higher frequencies ($\omega > 350$ GHz), the cyclotron resonance line splits into three lines F_1, F_2, and F_3 (Fig. 6). At low temperature, both F_2 and F_3 are weak. When the sample temperature is increased, the intensity of the line F_3 rapidly increases (Fig. 7). A plot of all the absorption lines positions is an $\omega(B)$ diagram is shown on Fig. 8.

We shall now show that this strange behavior can be qualitatively and quantitatively interpreted in terms of transitions between the forked Landau levels predicted by the theoretical model described in Sec. II (Fig. 9).

At low temperature and for our working frequencies, the quantum-limit condition $\hbar\omega_c \gg kT$ is realized. Only the lowest Landau levels ($n = 0^{\pm}$) are populated. All the F lines must be attributed to transitions from these levels to higher Landau levels.

At low frequency ($\omega \sim 130$ GHz), F corresponds to the transition from the degenerate states $n = 0^{\pm}$ towards the degenerate states $n = 1^{\pm}$ at $\omega = \omega_c = eB/m_c$ [cf. Eq. (7)]. When the magnetic field increases first the $n = 1^{\pm}$ levels, then the $n = 0^{+}$ levels split. Since the lowest Landau level 0^{+} has the highest hole population, the most intense line F_1 must be attributed to the allowed transition $0^{+} \rightarrow 1^{-}$.

The other allowed transition $0^{-} \rightarrow 1^{+}$ must lead to a weaker absorption peak at low temperature, since the 0^{-} level is less populated. However, since the energy separation between 0^{+} and 0^{-} is small, the intensity of this line should rapidly in-

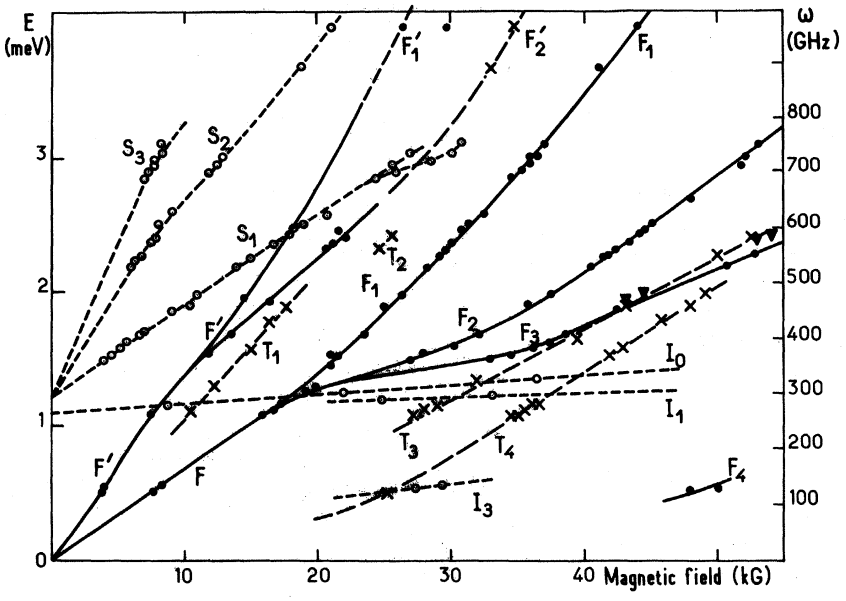

FIG. 8. Plot of the position of the transmission minima in the $\vec{B}$ parallel to bisector axis experiments: •, absorption lines observed at all temperatures; ○, absorption lines which disappear with increasing temperature; ×, lines observed at high temperature ($T>6$ °K).

crease with temperature. This is precisely the behavior of the F_3 line.

The F_2 line is fainter whatever the temperature; this suggests that it is to be attributed to the forbidden transition $0^+ \rightarrow 1^+$.

Finally, the F_4 line, which shows up at high magnetic field and low energy, can be interpreted as resulting from $0^+ \rightarrow 0^-$ transitions.

Plotting the observed lines in an $\omega(B)$ diagram (Fig. 8) thus gives precise information on the relative positions of the various Landau levels as a function of B, and the comparison with the energies computed within the theoretical scheme of Sec. II permits a determination of the model parameters. The best fit is obtained with

$$A = 63 \text{ meV},$$

$$\beta = \hbar^2/2m_{\parallel} = 4.63\hbar^2/m_c, \quad \text{corresponding to } m_{\parallel} = 0.108 m_0$$

$$\alpha = 5.566\hbar^2/m_0, \quad \text{corresponding to } m_{\perp} = (0.220 \pm 0.005) m_0 \tag{8}$$

$$t_0 = 2\alpha\zeta^2/A = 1.3, \quad \text{corresponding to } \Delta = A(t_0 - 1)^2/2t_0 = 2.18 \text{ meV}.$$

These values are entirely consistent with those obtained from magnetoabsorption experiments.[14] However, owing to our reevaluation of $m_{\perp}$, as compared with previous cyclotron resonance data (Picard, Mendum) used in (2), one should now take

$$\eta = -0.437 \quad \text{(instead of } \eta = -0.36).$$

And, for the lower valence band culminating at level H_5, the effective masses would then be

$$m_{l_2} = 0.039 m_0, \quad m_{t_2} = 0.256 m_0 .$$

The Landau levels which can be computed on this basis lead to the identification of all the other observed F lines. It thus appears that the secondary F' line is the second harmonic transition $n = 0 \rightarrow n = 2$. It splits at $B \sim 12$ kG, $\hbar\omega \sim 1.7$ meV into two lines $F_1'(0^+ \rightarrow 2^-)$ and $F_2'(0^- \rightarrow 2^+)$. Moreover, it becomes possible to explain the origin of an extra set of absorption maxima corresponding to the T lines.

T lines. At low magnetic field ($B < 20$ kG) an increase of temperature up to 10 °K causes holes to appear in the $1^{\pm}$ levels, thus permitting new transitions starting from these states. However, in this region, transitions $1^{\pm} \rightarrow 2^{\pm}$ occur at a frequency too close to that of the F line to result in an observable absorption peak. On the other hand, the predicted frequency for the $1 \rightarrow 3^+$ jump exactly corresponds to the T_1 line.

At higher fields ($B > 30$ kG) thermal excitation at temperatures $T > 25$ °K successively populates the 1^+ and 1^- levels; the transitions $1^+ \rightarrow 2^-$, $1^- \rightarrow 2^+$, and $1^+ \rightarrow 1^-$ are then possible. Their predicted positions correspond to the experimental lines, T_2, T_3, and T_4.

In conclusion, we have been able to identify all the transitions responsible for the F and T absorption lines, and to observe the splitting of the three first degenerate Landau levels $n = 0^{\pm}$ (at $B \sim 23$ kG), $n = 1^{\pm}$ ($B \sim 15$ kG) and $n = 2^{\pm}$ (at $B \sim 11$ kG). A general scheme of the calculated Landau levels and of the observed transitions is displayed on Fig. 9. Figure 10 shows a comparison between predicted and observed transitions.

B. Impurity Lines

In both directions $\vec{B} \parallel \vec{c}$ and $\vec{B} \perp \vec{c}$, the lines S_c and S_1 occur for a given magnetic field, at a transition

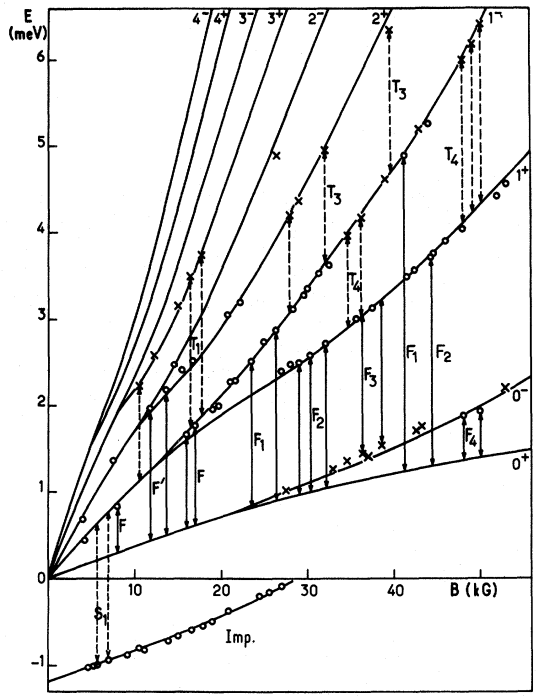

FIG. 9. General scheme of the energy levels for $\vec{B} \perp \vec{c}$ axis. The solid line gives the Landau levels as calculated using the parameter values of (8) in the text. All arrows are representative of a measured absorption maximum (the length of the arrow is equal to the microwave energy used in the corresponding experiment, its abscissa gives the magnetic field at the absorption peak). As can be seen, the transitions F_1 and F_2 from the O^+ level to the 1^- and 1^+ levels give experimental points in excellent agreement with theoretical prediction. Starting from these levels various transitions (F_4, F', T_1, T_3, T_4) also occur, all of which fit in quite well with the computed values of Landau energies up to $n=3$. Also shown below the origin is the fundamental impurity level responsible for the S_1 line.

energy equal to that of the main cyclotron lines (F_c and F) plus 1.24 meV. They shall consequently be ascribed to transitions to the $n=1$ level, from an impurity state located below the $n=0$ level, with an ionization energy $E_0 = 1.24$ meV.

In the same way for $\vec{B} \perp \vec{c}$, the weaker line S_2 is parallel to the F' line in the $\omega(B)$ plot; it will be attributed to a transition from the same impurity state towards level $n=2$ (more precisely, for magnetic field high enough to remove the degeneracy between 2^+ and 2^-, towards 2^+). The S_3 line can similarly be ascribed to a transition impurity $\rightarrow n=3$. The existence of impurity levels in tellurium is not surprising; even the purest samples of tellurium are all p type. There must be acceptor states close to the valence band. Thanh[20] made a calculation of the ionization energy for the ground state using the effective-mass approximation and found $E = 1.29$ meV which is in very good agreement with our result, as well as with magnetoabsorption data.[14]

In this case, the Fermi level is located between the acceptor level and the $n=0$ levels. As the temperature is raised, it gets nearer to the impurity band which rapidly depopulates. The intensity of the S lines decreases with temperature increase; they disappear at $T \sim 5$ °K.

To identify the nature of the acceptors in the purest samples, we performed experiments with samples voluntarily doped at $p \sim 10^{14}$ cm^{-3} either with bismuth or with antimony. In both cases the intensity of the S lines is much stronger than with pure samples, which fully supports our interpretation. The position of the lines observed with the bismuth-doped sample is identical to that observed in pure samples. The ionization energy is $E = 1.24$ meV. In the sample doped with antimony all lines are translated and extrapolate at zero magnetic field towards an ionization energy, which owing to a chemical shift, is reduced to $E \sim 1.16$ meV. This suggests that bismuth might be the remaining impurity of ultrapure samples.

I lines. The I lines in the $\omega(\beta)$ plot have a position which is almost field independent; the energy transition increases only slightly with B. The position of the lines I_0 and I_1 for $\vec{B}$ parallel to the bisector axis, as well as those of I_{c_0} and I_{c_1} for $\vec{B}$ parallel to the $\vec{c}$ axis extrapolate to a transition energy $E = 1.1$ meV at $B = 0$. The I_3 line extrapolates to $E = 0.22$ meV. The characteristic narrowness of these lines rules out the hypothesis that they could be attributed to transitions from impurity levels to a Landau level, because in such a case they would have the same broadness as the S lines. These lines are therefore to be ascribed to transitions from an impurity level to another impurity level. In particular, the lines I_0 and I_{c_0} can be associated with a transition from the fundamental impurity level (located 1.3 meV above the top of the valence band) to an impurity level located close (0.2 meV) to the valence band.

V. FURTHER TEST OF MODEL: CYCLOTRON RESONANCE IN MAGNETIC FIELD TILTED WITH RESPECT TO CRYSTALLOGRAPHIC AXES

As a means of checking the model, we performed experiments with the magnetic field parallel to the intermediate direction between the $\vec{c}$ axis and the bisector axis.

The experiments were carried out in the Voigt geometry with the sample plate parallel to the axial magnetic field of the superconducting coil. The sample could be rotated around its bisector axis so that any crystallographic direction of the surface between the $\vec{c}$ axis and the binary axis could be set parallel to the magnetic field. We shall call θ the angle of the magnetic field with the $\vec{c}$ axis, and φ

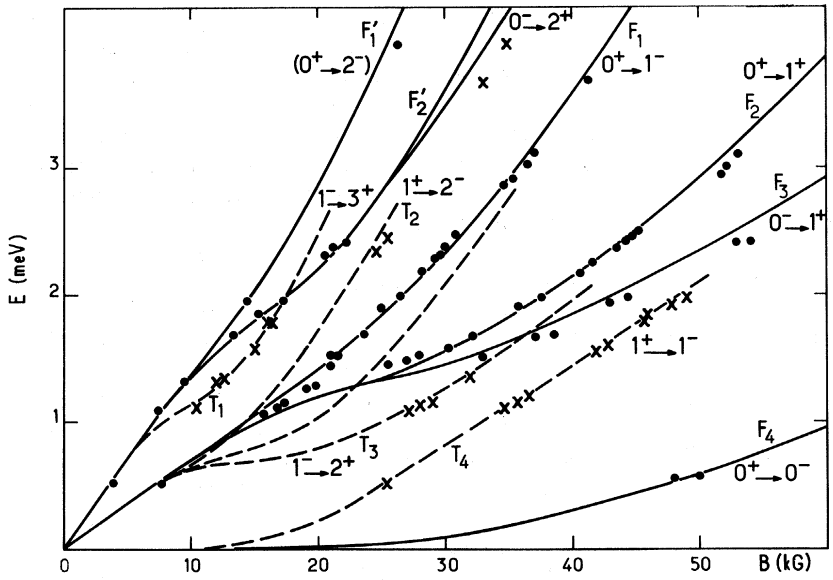

FIG. 10. $\vec{B} \perp \vec{c}$ axis. Scheme of the predicted transitions between the calculated Landau levels. Solid lines represent transitions from the lowest Landau levels $0^{\pm}$. Interrupted lines represent transitions from the higher energy levels $n = 1^{\pm}$. ●, experimentally observed transitions at $T = 1.5$ °K; ×, experimentally observed transitions at $T > 10$ °K.

$= \frac{1}{2}\pi - \theta$ the angle between the magnetic field and the binary axis. In the following, the discussion will be restricted to the main cyclotron resonance lines ($\Delta n = 1$).

At very low frequency ($\omega \sim 134$ GHz) the position of the magnetoplasma resonance $\omega = (\omega_c^2 + \omega_p^2)^{1/2}$ gives the value of ω_c. The observed cyclotron mass in the θ direction is very close to the mass m_c obtained for an ellipsoidal isoenergetic surface having a symmetry of revolution around the c axis (Fig. 11):

$$m_c = \left(\frac{\cos^2\theta}{m_{\parallel}^2} + \frac{\sin^2\theta}{m_{\parallel} m_{\perp}} \right)^{-1/2} , \tag{9}$$

with

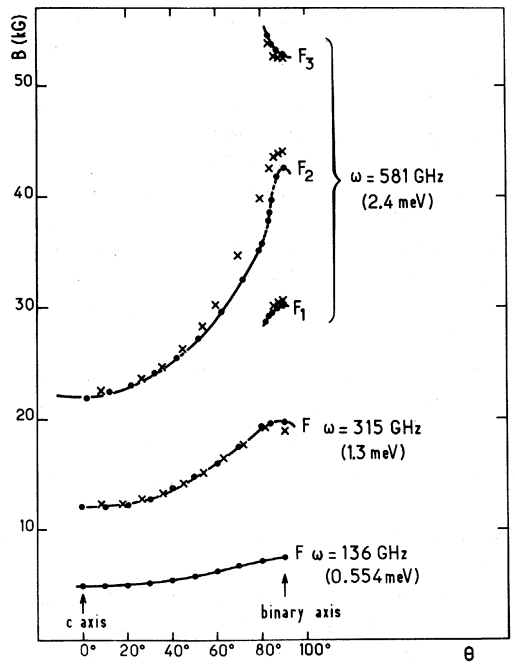

FIG. 11. Plot of the position of the fundamental cyclotron lines as a function of the angle θ ($\theta = \frac{1}{2}\pi - \varphi$) between the magnetic field and the $\vec{c}$ axis for three representative microwave frequencies. ●, experimental points; ×, calculated points.

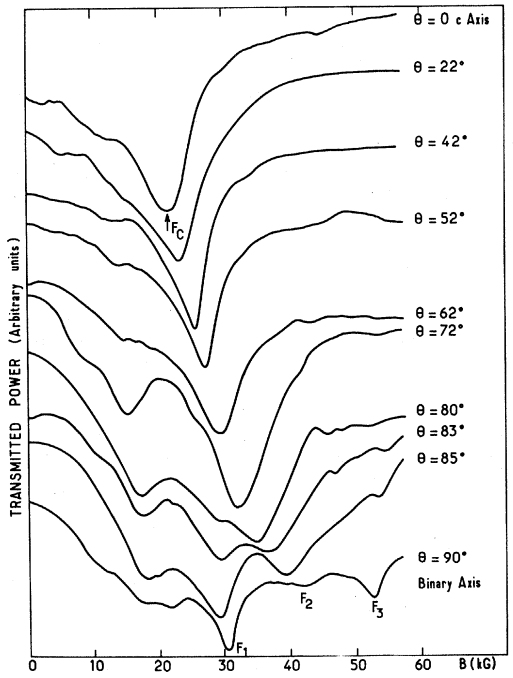

FIG. 12. Experimental recordings at a working frequency $\omega = 581$ GHz realized at temperature $T = 4.2$ °K by rotating the sample with respect to the magnetic field from a position with $\vec{B}$ parallel to the $\vec{c}$ axis ($\theta = 90° - \varphi = 0$) to a position with $\vec{B}$ parallel to the bisector axis ($\theta = 90°$).

$m_{\parallel} = (0.108 \pm 0.001)m_0$, $m_{\perp} = (0.220 \pm 0.005)m_0$.

At an intermediate frequency ($\omega \sim 315$ GHz) the position of the line agrees with this formula for angles $\theta < 40°$. For larger angles nonparabolicity effects become important and shift the line to a higher field.

Typical recordings for high frequencies ($\omega > 350$ GHz) can be seen on Fig. 12. The same shift is observed, in addition, for θ larger than a value $\theta_s \sim 82°$; two new lines F_1 and F_3 show up (Fig. 11). Their intensity rapidly increases with the increase of the angle, while the intensity of the central line F_2 weakens. For $\vec{B}$ parallel to the binary axis, the three lines F_1, F_2, and F_3 have the same position as observed in the Faraday configuration with $\vec{B}$ parallel to the bisector axis. As was noticed above, the F_2 line is weak because it corresponds to the forbidden transition ($0^+ \rightarrow 1^+$).

At very high frequency, $\omega \simeq 964$ GHz, an angular region appears between $\theta = 69°$ and 80°, where all the absorption lines broaden into a wide unresolved absorption.

All these features can be accounted for, within the model described in this paper, in the following fashion.

When the external magnetic field $\vec{B}$ is neither parallel nor perpendicular to the $\vec{c}$ axis, holes move in reciprocal space along quantized orbits situated in planes $k_B = \text{const}$, where k_B is the component of the wave vector $\vec{k}$ parallel to $\vec{B}$; such "orbital" planes are, of course, perpendicular to the magnetic field. For a given value of k_B, the Landau energies can be obtained, in the usual way, from the eigenvalues of a one-dimensional Hamiltonian describing a particle submitted to an "effective" potential $V(X)$. Apart from a B-dependent rescaling of the abscissa X and of the energies, $V(X)$ reproduces the variations of $E(\vec{k})$ in Eq. (2), with the $\vec{k}$ component parallel to the intersection of the considered orbital plane with the plane $k_y = 0$ which contains the $\vec{c}$ axis, the binary axis, and the magnetic field $\vec{B}$. The shape of the function $V(X)$ is readily obtained from the intersection curve of the surface $E(k_z, k_\perp)$ on Fig. 2 by a "vertical" plane making the angle φ with the k_z axis, which it touches at point $k_z = k_B/\sin\varphi$. (Such a curve is shown on Fig. 2 for a plane with $k_z = k_{z_0}$.)

For any orbital plane, it is then possible to evaluate the transition energy $\hbar\omega(\varphi, B, k_B)$ as the energy difference between the first Landau levels. The cyclotron resonance peaks will correspond to the transition energies for orbital planes which meet the following requirements.

(i) The transition energy for these planes must be extremal with respect to k_B (which means that there is an appreciable range of values of k_B for which the transition energy remains nearly constant, so that a number of neighboring orbital planes add their contributions to absorption at the considered microwave frequency).

(ii) The lower level involved in the transition must have a sufficient hole population.

For symmetry reasons, it is clear that the orbital plane $k_B = 0$ containing the origin in $\vec{k}$ space is always "extremal" in the sense defined in (i) above. But this plane, except for small values of φ, avoids the region surrounding the band minima where the hole concentration is high, so that it does not satisfy condition (ii).

On the other hand, and since holes are concentrated near the band minima ($k_z = \pm k_{z_0}$), condition (ii) is met by orbital planes with $k_B \simeq \pm k_{z_0} \sin\varphi$, which intersect the k_z axis near the band minima. Moreover, these planes are extremal for the two limiting cases $\varphi = 0°$ and 90°. This we shall take as an indication that they are at least nearly extremal for the intermediate values of φ. On these grounds, we are led to admit that the observed cyclotron resonance energies should essentially correspond to transition energies for orbital planes containing the valence-band minima.

The effective potential which then determines the Landau levels is shown on Fig. 13 for various values of φ. Starting from the symmetrical camelback curve for $\varphi = 0°$ ($\vec{B} \perp \vec{c}$ axis), one gets first an unsymmetrical graph with two potential wells, one of which corresponds to a secondary minimum (h'). For $\varphi \approx 16°$, this minimum vanishes, leaving a shoulder which progressively disappears; for $\varphi > 40°$, $V(X)$ is nearly parabolic.

The corresponding Landau levels are shown, as a function of the magnetic field, in Fig. 14. For $\varphi = 0°$ (dotted lines), one obtains the "forked" curves associated with levels $0^{\pm}$ and $1^{\pm}$ which have been abundantly discussed in Sec. IV.

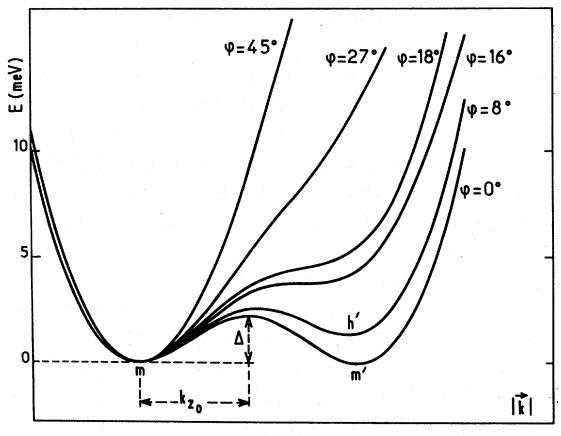

FIG. 13. Sketch of the effective potential for a hole moving in a magnetic field tilted by the angle φ from the bisector axis.

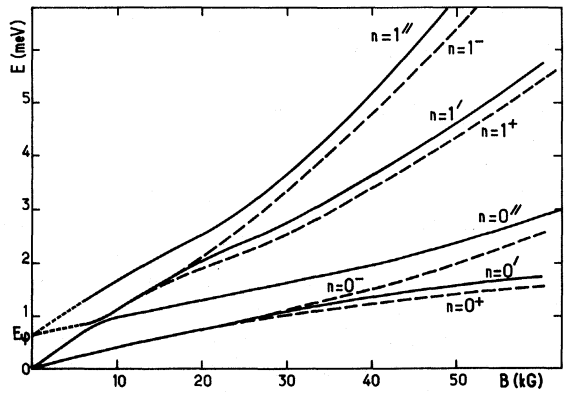

FIG. 14. Interrupted lines represent the first two Landau levels $n=0^{\pm}$ and $n=1^{\pm}$ for $\vec{B}$ parallel to the bisector axis. The solid lines show the first Landau levels for $\vec{B}$ at an angle $\varphi=6°$ from the bisector axis.

When φ increases, two sets of Landau levels appear (0′ and 1′, 0″ and 1″, shown for $\varphi=6°$ in Fig. 14). Two of them (0′, 1′) have zero energy for $B=0$, for sufficiently low magnetic field; they are associated to the main potential well around point m (Fig. 13). The other ones (0″, 1″) extrapolate at zero magnetic field to a finite energy E_φ which reproduces the energy of the secondary minimum around point h'; at low enough magnetic field, they are associated to the second potential well of $V(X)$. As a consequence, they disappear when φ becomes of the order of magnitude of 16°, that is when this secondary minimum is rubbed out. For higher values of φ, there remains only a single Landau ladder, which, at first, exhibits a somewhat irregular spacing of levels due to the nonparabolicity of $V(X)$; this feature is progressively removed as the magnetic field gets nearer to the c axis, and should no longer be present for $\varphi \gtrsim 40°$.

In addition, and for $\varphi \lesssim 16°$, increasing the magnetic field mixes levels which could initially be understood as describing particles confined either to the vicinity of m or to the neighborhood of h'. Such is certainly the case when the Landau energy is of the order of magnitude of the potential barrier between both minima. Our description can thus be put in correspondence with the results presented by other authors[15] using a semiclassical quantization argument.

The experimental results displayed on Fig. 11 can now be explained. At low microwave frequency (e.g., $\omega=136$ GHz), the transitions giving rise to cyclotron resonance take place between quantized orbits which, whatever the value of φ, are close to the band minima, where the isoenergetic surfaces are nearly ellipsoidal. The experimental data are thus in accordance with the conventional formula (9) (lower curve on Fig. 11).

At intermediate frequency (e.g., $\omega=315$ GHz), cyclotron resonance involves transitions between levels associated with the main effective potential well (0′ – 1′), but the nonparabolicity of $V(X)$ is now felt and formula (9) is no longer adequate. A numerical computation which takes into account this feature has been made and yields values of B at resonance which are in excellent agreement with experimental data (middle curve on Fig. 11).

At still higher frequency (e.g., $\omega=581$ GHz), and for $\varphi>16°$, the $B(\theta)$—or, equivalently, $B(\varphi)$—curve essentially reveals the nonparabolicity effects already discussed. For $\varphi<16°$, there appears the possibility of transitions between levels (0′, 1′) on one hand, and (0″, 1″) on the other, since, at the high magnetic fields which are now necessary to observe cyclotron resonance, all the Landau states spread over both hollows of the $V(X)$ curve. In addition to the F_2 (0′ – 1′) line, one thus gets a F_1 line (0′ – 1″) and a F_3 line (0″ – 1′), with still a fair agreement between computed and observed positions of the cyclotron resonance maxima (upper curve on Fig. 11).

On the whole, it appears that, from the quantitative as well as the qualitative points of view, the model we have proposed for the valence band of tellurium has been successfully checked by the whole set of experimental data that are now at our disposal.

VI. CONCLUSION

A careful study of cyclotron resonance in tellurium under various experimental conditions (microwave frequency, temperature etc.) has allowed a precise assignment of the observed absorption peaks to transitions between the Landau levels, which exhibit here a number of particular features owing to the nonparabolicity of the valance band, as for instance the "branching" of the main cyclotron resonance line. It has been possible to put forward a restricted set of band parameters, which lead to a quantitative agreement between computed and observed characteristics of the cyclotron resonance spectrum; these parameters are also compatible with the results of other experimental investigations (infrared absorption and magnetoabsorption, Shubnikov–de Haas effect). The model has further proved its validity by enabling us to bring into evidence some new features of cyclotron resonance: hitherto unnoticed lines for conventional orientation of the magnetic field with respect to the crystallographic axes, and modifications of the cyclotron resonance spectrum with a variable orientation of the magnetic field.

On the whole, it appears that, as regards its valence band, tellurium has one of the best-known band structures, and that by now further research efforts dealing with this material could well be de-

voted to other properties and characteristics.

ACKNOWLEDGMENTS

The authors wish to thank Dr. J. C. Picard who initiated these experiments; Professor J. Bok, Professor O. Betbeder-Matibet, Dr. A. Libchaber, and Dr. C. Rigaux for many stimulating discussions; J. Tuchendler who conceived and built the cyanide laser; and J. Brochard for his technical assistance.

---

*Laboratoire associé au Centre National de la Recherche Scientifique.

[1]J. H. Mendum and R. N. Dexter, Bull. Am. Phys. Soc. 9, 632 (1964).

[2]J. C. Picard and D. L. Carter, J. Phys. Soc. Japan, 21, 202 (1966).

[3]Y. Couder, Phys. Rev. Letters 22, 890 (1969).

[4]M. Picard and M. Hulin, Phys. Stat. Solidi 23, 363 (1967).

[5]D. Hardy and C. Rigaux, Sol. State Comm. 5, 889 (1967).

[6]O. Betbeder-Matibet and M. Hulin, Phys. Stat. Solidi 36, 573 (1969).

[7]W. Dreybrodt, K. J. Button, and B. Lax, Sol. State Comm. 8, 1021 (1970).

[8]W. Dreybrodt, M. H. Weiler, K. J. Button, B. Lax, and G. Landwehr, in *Proceedings of the Tenth International Conference on the Physics of Semiconductors, Cambridge, Mass.*, 1970, edited by S. P. Keller, J. C. Hensel, and F. Stein (U. S. AEC, Oak Ridge, Tenn., 1970), p. 347.

[9]R. Yoshizaki and Sh. Tanaka, J. Phys. Soc. Japan, 30, 1389 (1971).

[10]C. Guthmann and J. M. Thuillier, Phys. Stat. Solidi 38, 635 (1970).

[11]P. S. Dubinskaya, V. A. Noskin, I. G. Tagiev, I. I. Farbstein, and S. S. Shalyt, JETP Letters 8, 79 (1968).

[12]V. B. Anzin, M. S. Bresler, I. I. Farbstein, Yu. V. Kosichkin, and V. G. Veselago, Phys. Stat. Sol. 40, 417 (1970).

[13]D. Hardy and C. Rigaux, Phys. Stat. Solidi 38, 799 (1970).

[14]D. Hardy, C. Rigaux, J. P. Vieren, and Nguyen Hy Hau, Phys. Stat. Solidi 47, 643 (1971).

[15]M. S. Bresler and D. V. Mashovets. Phys. Stat. Solidi 39, 421 (1970).

[16]M. Hulin, in Ref. 8, p. 329.

[17]K. Nakao, T. Doi, and H. Kamimura, J. Phys. Soc. of Japan 30, 1400 (1971).

[18]M. H. Weiler, Sol. State Comm. 8, 1017 (1970).

[19]E. Bangert and W. Dreybrodt, Sol. State Comm. 10, 623 (1972).

[20]D. Thanh, Sol. State Comm. 9, 631 (1971).

[21]R. Yoshizaki and Sh. Tanaka, Sol. State Comm. 8, 1789 (1970).

[22]J. Ruvalds and J. W. McClure, J. Phys. Chem. Sol. 28, 509 (1967).

[23]R. V. Parfen'ev, A. M. Pogarskii, I. I. Farbstein, and S. S. Shalyt, Sov. Phys. Sol. State 4, 2620 (1963).

[24]Y. Couder and P. Goy, in *Microwave Research Institute Symposia Series*, edited by J. Fox (Interscience, New York, 1971), Vol. 20, p. 417.

[25]P. N. Robson, in *Coherent Sources using Electron Beams. Spectroscopic Techniques*, edited by D. H. Martin (North-Holland, Amsterdam, 1967), p. 261.

PHYSICAL REVIEW B VOLUME 7, NUMBER 10 15 MAY 1973

Test of the Virtual-Level Model of Dilute Alloys*

A. B. Callender† and S. E. Schnatterly‡

Joseph Henry Laboratories, Department of Physics, Princeton University, Princeton, New Jersey 08540

(Received 2 January 1973)

Measurements of the optical properties of dilute Ag : Pd alloys are described. The results are fitted to a calculation on the Friedel–Anderson model of the alloy. The agreement is sufficiently good that all of the free parameters of the model can be determined. Using these parameter values, other properties of the alloy are evaluated and compared with measurements, providing a test of the validity of the model. The result is generally favorable, and further work, both experimental and theoretical, can be done to make the test even more quantitative.

I. INTRODUCTION

The electronic structure of dilute transition-metal–noble-metal alloys has for many years been described by the Friedel–Anderson model.[1] This model has been used as a basis both for comparison with experimental results and for further theoretical work.[2]

In spite of the extensive use of the model, it has never been directly tested. That is, no experiment or experiments have been performed at low concentration which overdetermine the free parameters of the model to serve as a self-consistency check. The fundamental reason for this is that the usual quantities measured, such as resistivity, specific heat, and thermoelectric power, are each